Prepared for submission to JHEP

Draft: Constraints on Simplified Dark Matter Models using Mono-X Collider Searches

Amelia J. Brennan,[a,1] **Johanna Gramling,**[b] **Thomas Jacques,**[b] **and Millie F. McDonald**[a]

[a] *The University of Melbourne, Parkville 3010, Australia*

[b] *Université de Genève, Quai E. Ansermet 24, 1211 Genève 4, Switzerland*

E-mail: a.brennan@student.unimelb.edu.au, johanna.gramling@cern.ch, thomas.jacques@unige.ch, milliem@student.unimelb.edu.au

Abstract: Abstract...

[1] Corresponding author.

Contents

1 Introduction

Simplified models have emerged as a powerful tool for the interpretation of collider, direct and indirect detection signals of dark matter (DM). Previously, searches for DM were conducted within the context of both Effective Field Theories (EFTs) [1, 4–7, 30, 31] and full UV-complete theories like Supersymmetry [8, 10–12, 38] and extra dimensions []. The latter approach, though well-motivated, is typified by a broad parameter space and generally yields results which are insensitive to the wider class of DM models. EFT constraints, in comparison, are applicable to a broad range of models and rely on the specification of only a small set of parameters, namely the suppression scale, $M_\star$ and the DM mass, m_χ []. In the EFT framework, interactions between the dark and Standard Model (SM) sector are parametrised by a set of higher-dimensional effective operators []. These operators arise when the mass of the mediating particle is assumed to be significantly larger than the momentum transferred in a given interaction []. Where this is not the case, the EFT prescription can produce constraints which detour dramatically from those of the associated UV-complete model [22–26]. This is not so important in direct detection experiments where the momentum transferred in the scattering of DM particles with heavy nuclei is generally of the order of tens of keV [13, 14]. Similarly, in indirect searches the annihilations of non-relativistic DM particles in the galactic halo occur with momentum transfers on the order of m_χ []. However, for collider searches, where the accessible center of mass energy of two colliding baryons may be sufficient to produce the mediator on-shell, the range of validity of the EFT approach is significantly diminished []. Indeed, recent works ([]) have shown the EFT approach to be unreliable in some cases for the $\sqrt{\hat{s}} = 8$ TeV Run I of the Large Hadron Collider (LHC). Furthermore, the problem is expected to worsen in the current 13/14 TeV Run II. So, to accurately probe this regime, we move to Simplified Models [16].

In a nutshell, a simplified model arises when the heavy mediator which was integrated out in the EFT framework is reintroduced. Like EFTs, simplified models admit the comparison of results obtained in the different avenues of dark matter study [] and are defined by a relatively small set of parameters - namely m_{DM}, the mass of the mediator, $Mmed$, and the SM-mediator and DM-mediator coupling strengths, g_q and g_χ. Unlike EFTs, constraints calculated within the context of a simplified model are valid across a broad energy range ($\mathcal{O}$(GeV-TeV)).

To date, very few analyses include a dedicated study of any simplified models of DM. This is generally because the focus in DM collider searches at both ATLAS and CMS has been on generic EFT models. The recent release of several reports and recommendations on simplified models for the LHC [DM forum report, other SiMs paper] indicate that they are expected to play a more prominent role in Run II. The aim of this work, then, is to investigate a phenomenologically distinct set of simplified models likely to be included in Run II searches, and to constrain these using results already publicly available. In particular, constraints are placed on the simplified models corresponding to the simplest UV-completions in the s-channel of the D5 (vector) and D8 (axial-vector) effective operators[1]. We also

[1]The D5 and D8 operators form a nice starting point in the analysis of simplified models as they have

include a case with mediator exchange in the t-channel, which approaches the vector EFT model in the heavy-mediator limit, but remains kinematically distinct from its s-channel counterpart.

We constrain these models using public results from mono-X + missing transverse energy ($E_{\mathrm{T}}^{\mathrm{miss}}$) searches conducted by the ATLAS Collaboration. In particular, we focus on searches where X is either a parton (appearing as a narrow-radius jet), a leptonically-decaying Z boson, or a hadronically-decaying W or Z boson (appearing as a large-radius jet). The purpose of this approach is both to enhance and update existing simplified model limits [], using the full 20.3 fb^{-1} of Run I ATLAS data, and extend the range of phase space considered both in mass and relative strength of the couplings to the SM and DM sectors. We also aim to provide a cross-check and comparison of the performance of the three channels; while the mono-jet channel is expected to be most sensitive, the inclusion of two additional channels could enhance the limits in combination. Further, we extend the study of simplified models by allowing the width of the mediator and the SM-/DM-mediator couplings to vary, which previously have often been treated as fixed quantities []. We also include a comparison of collider limits with relic density constraints and limits from direct detection experiments.

The remainder of the paper is organised as follows. Section 2 contains a compendium of the simplified models chosen for analysis. Section 3 outlines the technique used to convert mono-X + $E_{\mathrm{T}}^{\mathrm{miss}}$ limits on the visible cross-section for any new physics process into constraints on simplified models, specifically, the couplings g_q and g_χ. Lastly, the results are presented in Section 4 along with a discussion of the implications of this work. Appendices A and B cover the details of our limit setting procedure and analyses validation.

2 Simplified models of dark matter

We begin with a short set of assumptions: that the DM particle, χ, is a weakly interacting Dirac fermion, that it is a singlet under the SM, and that it is the lightest stable new particle. We also require minimal flavour violation (MVF) to hold wherever relevant. Each model is built around a scenario whereby χ and SM quarks are coupled via a mediator. Coupling to SM leptons [] or gluons [] is beyond the scope of this paper, but these cases have been studied elsewhere. Resolving the $q\bar{q} \to \chi\chi$ contact interaction of an EFT at tree-level leads to two possibilities: exchange of the mediating particle in the s- or t-channel. In the former case, the mediator is also a SM singlet and is denoted ξ; in the latter it is necessarily charged and coloured, and is denoted ϕ. With these assumptions in mind, two s-channel models and one t-channel model were chosen for analysis.

The s-channel models are characterised by vector (sV) or axial-vector (sA) couplings to both the dark and SM sectors. In the notation of Ref. [23], these correspond to the

been studied exhaustively in the past (see Ref. []). This attention is motivated by the fact that collider limits for the D5 (D8) operator can be readily transformed into limits on spin-independent (spin-dependent) DM-nucleon scattering and vice versa. With the exception of D1 (see sec. **??**), and D9 and D11 (which have no simple simplified model counterparts []), the remaining effective operators induce elastic scattering which is suppressed by powers of the DM velocity or the momentum transferred [17]. Hence, these operators are largely ignored in the literature.

D5 and D8 operators respectively in the EFT regime. These models are described by the following interaction Lagrangians:

$$\mathcal{L}_{sV} = -\xi_\mu \left[\sum_q g_q \bar{q} \gamma^\mu q - g_\chi \bar{\chi} \gamma^\mu \chi \right], \tag{2.1}$$

$$\mathcal{L}_{sA} = \xi_\mu \left[\sum_q g_q \bar{q} \gamma^\mu \gamma_5 q - g_\chi \bar{\chi} \gamma^\mu \gamma_5 \chi \right], \tag{2.2}$$

where the sum is over all quarks. For the couplings g_q and g_χ to remain within the perturbative regime, they are required to satisy $g_q, g_\chi \leq 4\pi$, though stronger perturbativity requirements do exist [15].

The last model considered in this paper, a t-channel scalar mediator model (which we refer to by the descriptor tS), juxtaposes nicely with the s-channel models. In the heavy-mediator limit, it is converted into a combination of the D5 and D8 EFT operators via Fierz transformation. In addition, the tS model is motivated by analogy with a common aspect of Supersymmetric models: neutralino DM interacting with the SM sector via t-channel exchange of a squark[2] [18].

In this model, the mediator which we call ϕ necessarily has colour charge, and can couple to either the left or right-handed quarks as a SU(2) doublet or singlet respectively. Since the LHC is insensitive to the chirality of the quarks, for simplicity we assume that the mediator couples to the left-handed quarks only, that the masses and couplings of ϕ are equal across the three generations, and that the masses of the two components of ϕ are equal. The interaction Lagrangian for this model is then:

$$\mathcal{L}_{int} = \sum_Q g_{q\chi} \bar{Q} P_R \phi \chi + \text{h.c.}, \tag{2.3}$$

where the sum is over the three Q_L doublets, $g_{q\chi}$ is the scalar coupling of the incoming quark, ϕ and χ, and P_R is the usual chiral projection operator.

2.1 Mass and Coupling Points

We choose to study a representative set of dark matter and mediator masses, shown in Table 1. DM masses of 3, 30 and 300 GeV are only included in the mono-Z channel. All $m_\chi - M_{\text{med}}$ combinations are permitted in the sV and sA models; in the tS model M_{med} should be greater than m_χ, to ensure stability of the DM particle. The couplings, g_q and $g_{q\chi}$, are set to unity while the DM-mediator coupling, g_χ, is allowed to vary from this by up to a factor of five for the s-channel models. In all cases, a point in phase space is disregarded if it leads to a mediator width greater than 50% of the mediator mass, as will be further discussed below. The mediator masses were chosen to cover a broad range

[2] Note that in the Supersymmetric scenario the DM particle is a Majorana fermion. Simplified models in which the DM particle is a Majorana fermion are not covered here (the exception being in the validation of the mono-Z channel, see sec.B.2) as they are kinematically identical to the corresponding Dirac cases, and only require multiplication of the cross-section by a simple factor in order to calculate limits. The exception to this rule is the s-channel vector mediator model, which vanishes if χ is a Majorana fermion [19].

m_χ [GeV]	M_{med} [GeV]	s-channel		t-channel
		g_q	g_χ	$g_{q\chi}$
1, (3), 10, (30), 100, (300), 1000	1, 2, 10, 20, 100, 200, 1000, 2000, 20 000	1	0.2, 0.5, 1, 2, 5	1

Table 1: Mass and coupling points chosen for the analysis of simplified dark matter models. Values in brackets are only included in the mono-Z channel. The mediator masses are primarily representative of three regimes: (near-)degenerate ($M \approx m_\chi$), kinematically allowed ($M \geq 2m_\chi$), and EFT-like ($\sqrt{\hat{s}} << M$). Coupling values that give a mediator width such that $\Gamma_{\text{med}} > 0.5 \times M_{\text{med}}$ are not considered. For the t-channel model, $M_{\text{med}} > m_\chi$ is also required.

of parameter space and to coincide with predominantly three regimes: (near-)degenerate ($M \approx m_\chi$), kinematically allowed ($M \geq 2m_\chi$), and EFT-like ($\sqrt{\hat{s}} << M$)[3]. We also allow for the possibility of a light mediator/heavy WIMP scenario (M $< m_\chi$) in the sV and sA models.

2.2 Width effects

An important factor when considering simplified models is to ensure the mediator width is treated appropriately, as it impacts both the cross-section calculation and, in some cases, the kinematic behaviour of the model. In previous analyses (ref) it has been common to consider mediators of a fixed width such as $\Gamma = M/8\pi$ (the minimal width possible with only a single quark helicity coupling to the mediator with $g_q = 1$), to take advantage of the enhancement in cross section as the width becomes small and on-shell.

In this work, the mediator widths are expanded to include coupling to all kinematically accessible quarks. We assume minimal flavour violation, which implies a universal coupling to all quark flavours. Following [(other minimum width papers)], the minimum on-shell kinetic width for each model is given by:

$$\begin{aligned}\Gamma_{sV} &= \frac{g_\chi^2 M}{12\pi}\left(1+\frac{2m_\chi^2}{M^2}\right)\left(1-\frac{4m_\chi^2}{M^2}\right)^{\frac{1}{2}}\Theta(M-2m_\chi) \\ &\quad + \sum_q \frac{g_q^2 M}{4\pi}\left(1+\frac{2m_q^2}{M^2}\right)\left(1-\frac{4m_q^2}{M^2}\right)^{\frac{1}{2}}\Theta(M-2m_q)\end{aligned} \tag{2.4}$$

[3]A recent study by Alves et al. found that EFT results do not apply to mediators with a mass less than 2.5 TeV at the LHC during Run I [33].

$$
\begin{aligned}
\Gamma_{sA} &= \frac{g_\chi^2 M}{12\pi}\left(1-\frac{4m_\chi^2}{M^2}\right)^{\frac{3}{2}}\Theta(M-2m_\chi) \\
&\quad + \sum_q \frac{g_q^2 M}{4\pi}\left(1-\frac{4m_q^2}{M^2}\right)^{\frac{3}{2}}\Theta(M-2m_q)
\end{aligned}
\tag{2.5}
$$

$$
\begin{aligned}
\Gamma_{tS} &= \sum_q \frac{g_{q\chi}^2 M}{16\pi}\left(1-\frac{m_q^2}{M^2}-\frac{m_\chi^2}{M^2}\right) \\
&\quad \times \sqrt{\left(1-\frac{m_q^2}{M^2}+\frac{m_\chi^2}{M^2}\right)^2-4\frac{m_\chi^2}{M^2}}\;\Theta(M-m_q-m_\chi)
\end{aligned}
\tag{2.6}
$$

The expressions for width above are valid where that width is smaller than the mass of the mediator. Moreover, a recent paper [Tom+Karl, others?] demonstrated that the MadGraph treatment of the mediator as a Breit-Wigner propagator, rather than a true kinetic propagator, is accurate only up to $\Gamma \lesssim M/2$. This was also shown to be a necessary requirement for the following approximations regarding the relationship between the couplings and the cross section to hold:

$$
\sigma \propto \begin{cases} g_q^2 g_\chi^2/\Gamma & \text{if} M_{\text{med}} \geq 2m_\chi \\ g_q^2 g_\chi^2 & \text{if} M_{\text{med}} < 2m_\chi \end{cases}
\tag{2.7}
$$

in the sV and sA models, and

$$
\sigma \propto g_{q\chi}^4
\tag{2.8}
$$

in the tS model. We find that this requirement fails for a subset of the phase space in the sV and sA models[4], and therefore do not include such points in this work. The impact of varying the mediator width is demonstrated in Fig 1. For the sV and tS models, we plot a simplified $E_{\mathrm{T}}^{\mathrm{miss}}$ distribution, as a proxy for the full selection in each analysis, for two and three demonstrative mass points and couplings respectively. The strength of the coupling directly impacts the width of the mediator in each case. In the mono-Z channel[5], the $E_{\mathrm{T}}^{\mathrm{miss}}$ distribution is predominantly independent of the mediator width, and this is also true for the sV model in the mono-jet channel. However, there is a clear variation in kinematic behaviour in the tS model in the mono-jet channel, which can be attributed to additional diagrams with a gluon in the initial state, accessible in the mono-jet channel, which allow the mediator to go on-shell. In this scenario, when the resulting quark and DM particle are both small compared to the mediator mass, they share equally its energy leading to a peak in the $E_{\mathrm{T}}^{\mathrm{miss}}$ distribution at approximately half the mediator mass.

[4]Note that the t-channel widths are consistently narrower than their s-channel counterparts, as there are six independent mediators compared to the single s-channel model mediator.

[5]In this discussion, the mono-W/Z channel can be assumed to follow the same logic as for the mono-Z channel.

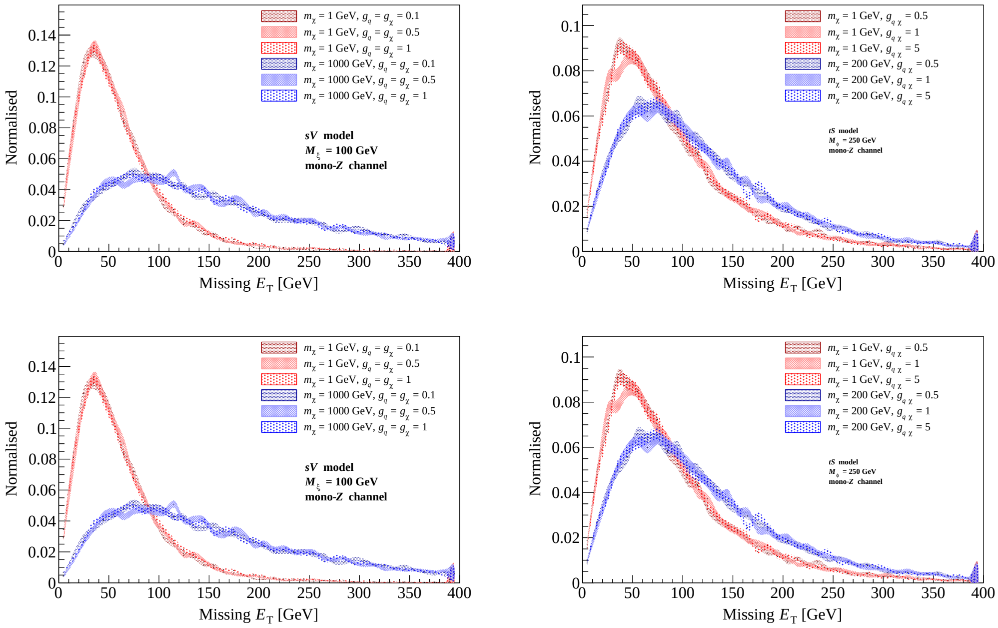

Figure 1: The E_T^{miss} distribution showing the lack of dependence on the coupling (and hence the width) - possibly should include the widths on the plot. Top plots should be replaced with mono-jet case.

In the cases where the model behaviour is independent of the width, we can greatly simplify the calculations by assuming the effect of selection cuts in each channel is constant for each masspoint; that is, independent of the couplings. In this case, a simple rearrangement of eqns. 2.7 and 2.8 allows us to obtain upper limits on the model couplings (see App. A for further details of this calculation).

Studies of the tS model within the mono-jet channel, where scaling the coupling can lead to changed kinematic behaviour, have been performed elsewhere [Papucci], and require the use of iterating the couplings during sample generation. This, combined with the challenges of including differing orders of α_s in the mono-jet channel, make the generation process highly computationally expensive compared to the mono-Z and mono-W/Z channels, and so we do not consider that particular case here.

3 Recasting mono-X constraints

The mono-X + E_T^{miss} (abbreviated mono-X) signal is a popular collider signal in the search for new physics, particularly in the search for dark matter. Since WIMPs are not expected to interact with detector material, they appear as missing transverse momentum, $\vec{p}_T^{miss}$, when balanced against a visible object that is radiated from the initial or intermediate state. For the s-channel simplified models discussed in Section 2, a SM particle, X, is emitted from one of a pair of intial-state partons (shown in Figure **??**). The case where X is radiated from the mediator - a process known as virtual internal Bremsstrahlung - is only possible if the SM-dark matter interaction occurs via the t-channel (as shown in Figure **??**). For all models, emission of a parton is the most likely scenario at the LHC owing to the strength of the strong coupling. Hence we focus on the mono-jet channel as it is expected to provide the strongest limits. Emission of Z and W bosons or photons is also possible however, and may be chosen for study over jet processes to take advantage of the relative simplicity of leptons compared to jets. As such, we also include the mono-$Z(\to \ell^+\ell^-)$ channel for comparison. Finally, we extend this work by including the hadronically-decaying mono-W/Z channel for comparison.

The procedure for recasting existing mono-X constraints as simplified model constraints is straightforward. Firstly, signal events are simulated as described in Section 3.1. The event selection criteria of the mono-X analysis of interest is then reproduced and applied to the simulated signal samples. Events surviving the selection criteria are counted to determine both the likelihood of a dark matter event occurring (referred to as the acceptance, $\mathcal{A}$) and the probability of detecting said event (refered to as the efficiency, ϵ). These quantities are then used in combination with channel-specific model-independent limits on new physics events to limit the parameter phase space of a given model. For a comprehensive description of the recasting procedure, see appendix A.

In this paper, mono-jet constraints are derived from a search for new phenomena conducted by the ATLAS Collaboration using pp collisions at $\sqrt{s} = 8$ TeV as described in Ref. [39]. Similarly, the leptonic mono-Z and hadronic mono-W/Z constraints are derived from ATLAS dark matter searches originally optimised for the D1, D5 and D9 effective operators [45**?**]. These analyses are described in further detail in Sections 3.2, 3.3 and **??** respectively.

3.1 Signal Simulation

Signal samples for each channel and for each simplified model discussed in Section 2 were generated in the following manner. Firstly, leading order matrix elements for the process $pp \to \mathrm{X} + \chi\bar{\chi}$ (where X is either one or two jets[6], a $Z(\to \ell^+\ell^-)$ boson or a $W/Z(\to$ jets) boson) were modelled using MADGRAPH5_AMC@NLO v2.2.2 [46] with the PDF MSTW2008lo68cl [47]. The default renormalisation and factorisation scales were also used and set to the sum of $\sqrt{m^2 + p_T^2}$ for all particles in the final state. Showering and hadronisation were then performed by PYTHIA 8.201 with the appropriate PDF and using the ATLAS UE Tune AU2-MSTW2008LO [48]. The detector response was approximated by applying a gaussian smearing to the p_{T} of the leptons and jets. FastJet **??** was used to reconstruct small-radius jets (anti-kT algorithm with $R = 0.4$) for the mono-jet channel, and large-radius jets (Cambridge-Aachen algorithm with $R = 1.2$) for the mono-W/Z channel; the latter also uses a mass-drop filtering procedure as discussed at ref. **??**, with $\mu = 0.67$ and $y = 0.16$.

[6]For the monojet channel, jets are seeded by any parton excluding the (anti-)top quark.

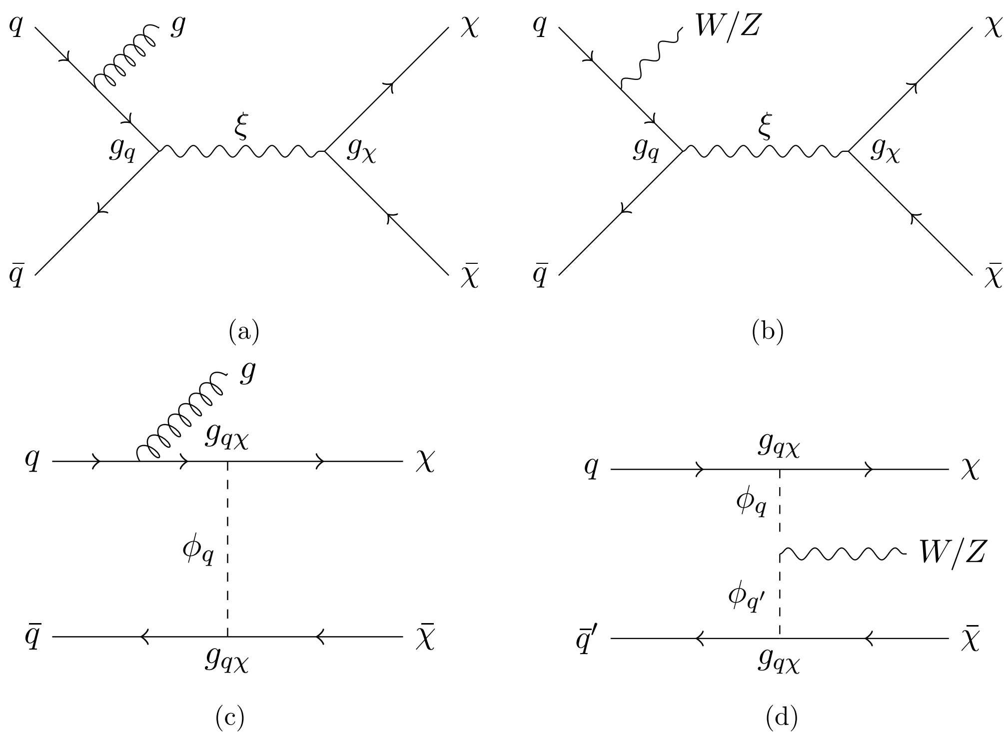

Figure 2: Representative dark matter pair-production processes with a gluon or a W or Z boson in the final state for the s-channel (a,b) and t-channel (c,d) models.

3.1.1 Parton Matching Scheme

For the mono-jet channel, matching of partons generated in MADGRAPH5 to jets generated in PYTHIA is performed using the MLM scheme, with a single matching scale (known as the QCUT). The use of a single matching scale initially seems problematic as the choice of QCUT can influence somewhat the distributions of p_{T} and $E_{\mathrm{T}}^{\mathrm{miss}}$. In particular, it leads to increased uncertainty in the case where the mediator mass is significantly larger that the QCUT value, due to the resulting lack of statistics. The ATLAS mono-jet analysis attempts to mitigate this effect with the creation of two subsamples, with different QCUT values, and merging these with a cut on the leading jet p_{T} to avoid double-counting. However, we found that use of a single QCUT value at 80 GeV was able to adequately reproduce the results of the ATLAS mono-jet analysis for the masses of interest, while substantially reducing both the complexity and computational expense of the mono-jet channel MC generation and systematic uncertainty estimation procedures (see section B.1).

We now move to a discussion of each of the mono-X channels separately.

3.2 Monojet Constraints

The ATLAS mono-jet plus missing transverse energy search [39] was originally designed to set limits on three new physics scenarios, the most relevant of which is the production of

WIMP DM within the context of seven (?) effective operators. The analysis also includes a brief study of a Z' DM model which is analogous to our sV model.

Signal selection is carried out based on at least one hard jet recoiling against missing energy. To ensure that the correct back-to-back jet + $E_{\mathrm{T}}^{\mathrm{miss}}$ topology is selected events are required to have a leading jet, j_1, with $p_T > 120$ GeV and $|\eta| < 2.0$ satisfying $p_T^{j_1}/E_{\mathrm{T}}^{\mathrm{miss}} > 0.5$. Surviving events must then satisfy $|\Delta\phi(j, \vec{E}_{\mathrm{T}}^{\mathrm{miss}})| > 1.0$, where j is any jet with $p_T > 30$ GeV and $|\eta| < 4.5$. This criterion reduces the multijet background contribution where the large $E_{\mathrm{T}}^{\mathrm{miss}}$ originates mainly from jet energy mismeasurement. Note that there is no upper limit placed on the number of jets per event. The contribution from the dominant background processes, W/Z+jets ([7]), is managed with a veto on events containing muons or electrons with $p_T > 7$ GeV. A further veto is placed on events containing isolated tracks[8] with $p_T > 10$ GeV and $|\eta| < 2.5$. This reduces the contribution from non-identified leptons (e, μ or τ) in the final state. Lastly, nine separate signal regions are defined with increasing lower thresholds on $E_{\mathrm{T}}^{\mathrm{miss}}$, which range from 150 GeV to 700 GeV as shown in Table 2.

The ATLAS mono-jet analysis revealed no significant deviation of observed events from the expected SM backgrounds in the Run 1 8 TeV dataset. Subsequently, limits on new physics signatures were derived in terms of the visible cross-section, $\sigma \times \mathcal{A} \times \epsilon$, using the HistFitter package []. These model-independent limits are shown in Table 2 and correspond to the 95% confidence level.

Signal Region	$E_{\mathrm{T}}^{\mathrm{miss}}$ threshold [GeV]	$\sigma \times \mathcal{A} \times \epsilon$ [fb]
SR1	150	726 (935)
SR2	200	194 (271)
SR3	250	90 (106)
SR4	300	45 (51)
SR5	350	21 (29)
SR6	400	12 (17)
SR7	500	7.2 (7.2)
SR8	600	3.8 (3.2)
SR9	700	3.4 (1.8)

Table 2: The ATLAS mono-jet $E_{\mathrm{T}}^{\mathrm{miss}}$ signal regions and corresponding observed (expected) model-independent upper limits on $\sigma \times \mathcal{A} \times \epsilon$ at 95% confidence level. Adapted from Ref. [39].

The Monte Carlo (MC) generation and event selection procedures discussed above were validated for the mono-jet channel via reproduction of ATLAS limits on the suppression scale, $M_\star \equiv M_{\mathrm{med}}/\sqrt{g_q g_\chi}$, for the Z' model. The details of this process are contained in appendix B.1. Importantly, we observe agreement within ~23% for all samples.

[7]Do I want to be more specific here? Eg. $W(\to \ell\nu)$+jets, $Z(\to \nu\bar{\nu})$+jets, $Z/\gamma^*(\to \ell^+\ell^-)$+jets?

[8]A track is considered isolated when no additional track with $p_T > 3$ GeV lies within a cone of radius 0.4 around it.

3.3 Mono-Z Constraints

The signature of the ATLAS mono-$Z(\to \ell^+\ell^-)$ analysis [45] is a pair of opposite-sign same-flavour leptons balanced against a large amount of missing transverse momentum. The analysis is designed to search for a set of EFT models of DM, where a Z boson is radiated from an initial state quark. Leptons are in general much cleaner and simpler than jets, so this channel is included here to investigate whether the reduction in systematic uncertainties can provide easily-obtained results that are comparable to the more complicated mono-jet channel.

The analysis also includes a short study of a t-channel simplified model similar to that discussed here. This model is used to validate our results in this channel; see the details in sec. B.2.

The selection is summarised as follows (see the paper for a full description). Electrons (muons) are required to have a p_{T} greater than 20 GeV, and $|\eta|$ less than 2.47 (2.5). Two opposite-sign, same-flavour leptons are selected, and required to have invariant mass and pseudorapidity such that $m_{\ell\ell} \in [76, 106]$ GeV and $|\eta^{\ell\ell}| < 2.5$. The reconstructed Z boson should be approximately back-to-back and balanced against the $E_{\mathrm{T}}^{\mathrm{miss}}$, ensured with the selections $\Delta\phi(\vec{E}_{\mathrm{T}}^{\mathrm{miss}}, p_{\mathrm{T}}^{\ell\ell}) > 2.5$ and $|p_{\mathrm{T}}^{\ell\ell} - E_{\mathrm{T}}^{\mathrm{miss}}| \,/\, p_{\mathrm{T}}^{\ell\ell} < 0.5$. Jets are reconstructed with the anti-k_t algorithm, with radius parameter 0.4; events containing a jet with $p_{\mathrm{T}} > 25$ GeV and $|\eta| < 2.5$ are vetoed. Events are also vetoed if they contain a third lepton with $p_{\mathrm{T}} >$ 7 GeV. The signal regions are defined by increasing lower $E_{\mathrm{T}}^{\mathrm{miss}}$ thresholds: $E_{\mathrm{T}}^{\mathrm{miss}} > 150$, 250, 350, 450 GeV.

The dominant background in this analysis is the irreducible $ZZ \to \ell^+\ell^-\bar{\nu}\nu$ process, which has a softer $E_{\mathrm{T}}^{\mathrm{miss}}$ distribution that the DM signal. The background is estimated with MC simulation, and has a systematic uncertainty in the range 36-46% across the four signal regions.

A cut-and-count strategy is used, and the total numbers of expected and observed events, along with total uncertainties, are reported for each signal region. The published result unfortunately does not give upper limits on the number of new physics events, so we calculate these ourselves: we obtain upper limits on $N_{exp,obs}$ (see eq. A.1) with a simple implementation of HistFitter that uses a frequentist calculator and a one-sided profile likelihood test statistic (the LHC default), giving the model-independent upper limits shown in table **??**. Note that we use signal regions 1 and 2 only, as this simplified HistFitter approach was deemed inappropriate for the very low statistics of signal regions 3 and 4. These upper limits are also used for our validation procedure (see sec. B.2).

3.4 Mono-WZ Constraints

Note to Johanna: Here you should discuss the original intention of the mono-W analysis. Also comment on any validation you did in order to confirm that you could use the results of the analysis. Lastly, discuss or list the cuts used in the analysis and the uncertainties associated with the results. This will inevitably include details of the background estimation and the detector performance.

	SR1 ($E_T^{miss} > 150$ GeV)	SR2 ($E_T^{miss} > 250$ GeV)
N_{sig}^{exp}	34.7	6.8
N_{sig}^{obs}	32.2	5.9

Table 3: The expected and observed upper limits on the number of new physics events in the ATLAS mono-Z analysis, calculated with HistFitter using the results of [45].

The analysis focusing on fully-hadronic decays of the bosons in the mono-W/Z channel performed by ATLAS on the 8 TeV dataset was considered especially interesting, since a constructive interference in the mono-W channel for the vector operator in EFT models was assumed possible, leading to limits even stronger than the ones from monojet searches in this case. By now, studies have revealed that such a scenario would violate unitarity and this interpretation is not emphasised in this work due to these concerns.

Nevertheless, this channel is an interesting addition, since it exploits the large branching fraction of hadronic boson decays. Also, the experimental techniques applied are significant different, the selection is based on large-R jets that are consistent with the hypothesis of coming from an EW boson. In addition, large missing ET is required, as for all monoX searches.

The applied event selection is summarised in the following: electrons, muons and photons are vetoed if their p_T is larger than 10 GeV and they are within $|\eta|$ ¡ 2.47 (electrons), 2.5 (muons), 2.37 (photons). Large radius jets are jets reconstructed with the Cambridge-Aachen algorithm using $R = 1.2$. A mass drop filter is applied and $\sqrt{y} > 0.4$[9] is required in order to suppress non-W/Z processes. Events with at least one large radius jet with p_T ¿ 250 GeV, $|\eta|$ ¡ 1.2 and with a mass in a window around the W/Z mass, between 50 and 120 GeV, are selected. To reduce ttbar and QCD background, events containing small-R jets (anti-k_T, R = 0.4) with $\Delta\phi(jet, E_T^{miss}) < 0.4$ or more than one jet (p_T ¿ 40 GeV, $|\eta|$ ¡ 4.5) with $\Delta R(jet, large - Rjet) > 0.9$ are vetoed. The original analysis considers two signal regions: $E_T^{miss} > 250 GeV$ and $E_T^{miss} > 500 GeV$. We consider in the following only the signal region with $E_T^{miss} > 500 GeV$.

The main background is coming from $Z \to \bar{\nu}\nu$ events that have additional jets coming from initial state radiation. Further important backgrounds from W/Z+jets events, in which W/Z decays leptonically, enter the selection if the lepton(s) is missed due to being out of acceptance or failing ID requirements, or in case it is a hadronically decaying tau. All these backgrounds are estimated in dedicated control regions.

Whereas the ATLAS analysis uses a shape fit of the mass distribution of the large radius jet, we just regard the number of events in the signal region, since the data points of the m_{jet} distribution were not published. check!!!

From the published number of expected and observed events in the signal region and their uncertainties, we calculate the upper limit on the number of new physics events as

[9] momentum balance of the two leading subjets, $\sqrt{y} = min(p_{T1}, p_{T2})\Delta R/m_{jet}$

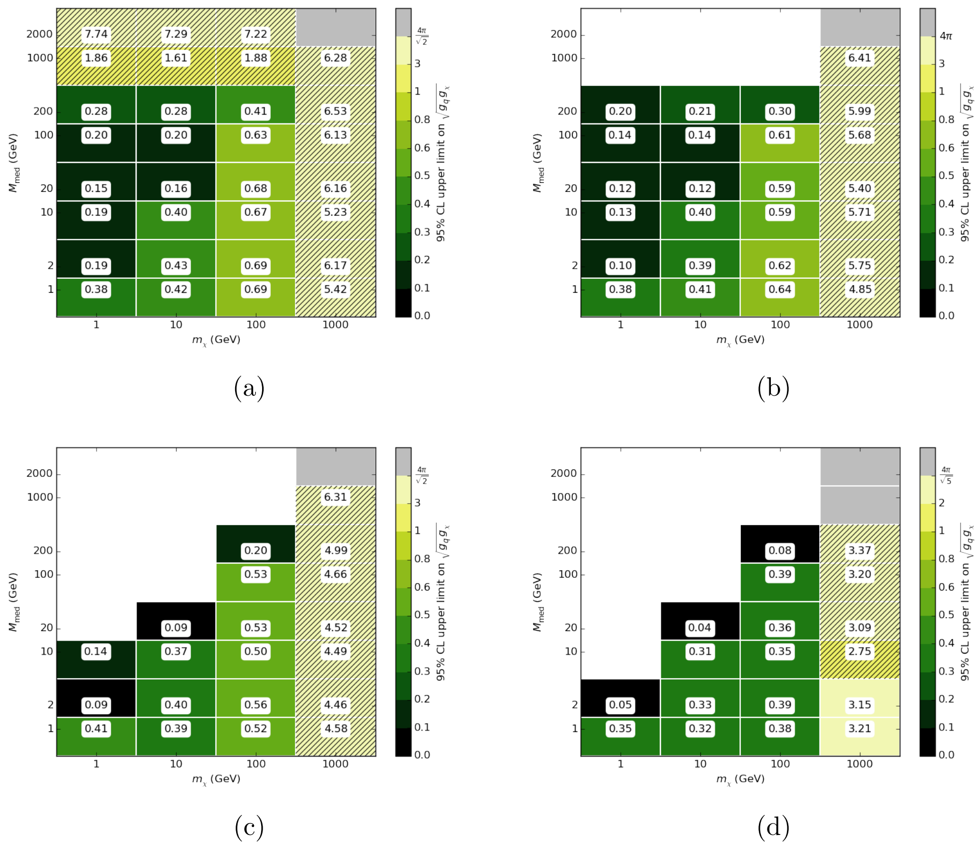

Figure 3: Upper limits on the coupling for the sV model, in the mono-jet channel, for $g_\chi/g_q = 0.5$ (a), 1 (b), 2 (c) and 5 (d). The grey region represents the phase space where no meaningful limit was obtained. The hatched region represents a limit which leads to a width greater than $M_{\text{med}}/2$, so the validity of the calculation begins to fail.

described above for the mono-Z channel (see eq. A.1). We obtain the following numbers: $N_{exp} = 27.2$, $N_{obs} = 27.4$.

4 Limits on the coupling $\sqrt{g_q g_\chi}$

The 95% confidence level upper limits on the couplings $\sqrt{g_q g_\chi}$ of the sV and sA models, and $g_{q\chi}$ of the tS model, obtained from each of the mono-X channels, are presented in figs. ref. These quantities are evaluated as described in appendix **??** and correspond to the best limits of each signal region tested.

Some general comments here. Note removal of $g_\chi/g_q = 0.2$.

The results are discussed below.

4.1 Mono-jet channel

Results discussion here.

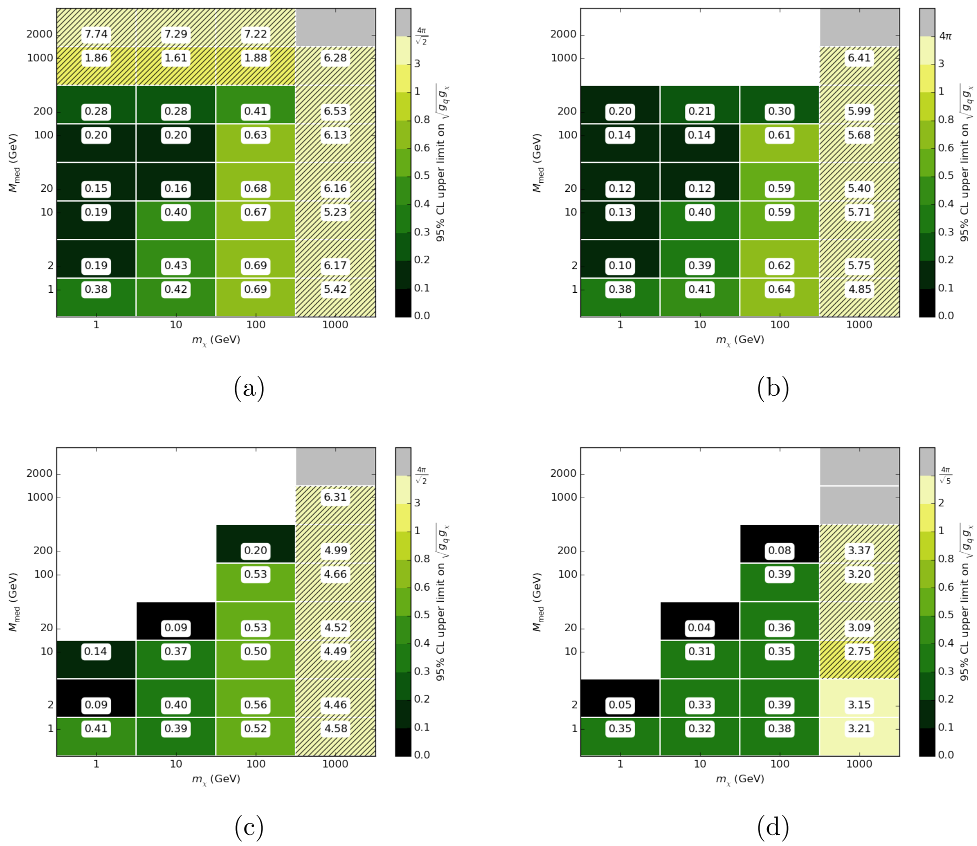

Figure 4: Upper limits on the coupling for the sA model, in the mono-jet channel, for $g_\chi/g_q = 0.5$ (a), 1 (b), 2 (c) and 5 (d). The grey region represents the phase space where no meaningful limit was obtained. The hatched region represents a limit which leads to a width greater than $M_{\rm med}/2$, so the validity of the calculation begins to fail. TO BE UPDATED WITH sA PLOTS.

4.2 Mono-Z channel

Mono-Z limits discussion here. Overall uncertainty on $\sqrt{g_q g_\chi}$ generally $< 10\%$, up to 80%.

4.3 Mono-W/Z channel

Mono-W/Z limits discussion here.

5 Conclusion

5.1 Comparison with Relic Density Constraints

In Figs. **??** we show lines where the constraint on the coupling corresponds to the coupling strength that would reproduce the correct DM density if DM is a thermal relic of the early universe. For points above the line, the LHC constraints naively rule out the couplings leading to the correct relic density. Below this line the relic density coupling is still allowed.

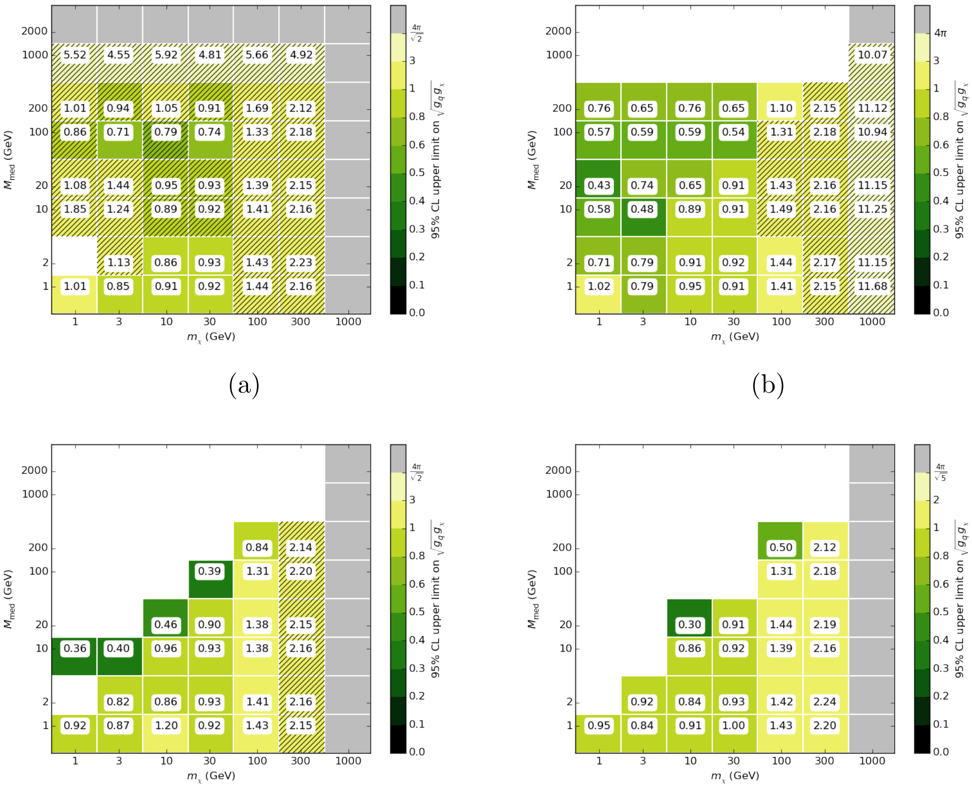

(a) (b) (c) (d)

Figure 5: Upper limits on the coupling for the sV model, in the mono-Z channel, for $g_\chi/g_q = 0.5$ (a), 1 (b), 2 (c) and 5 (d). The grey region represents the phase space where no meaningful limit was obtained. The hatched region represents a limit which leads to a width greater than $M_{\rm med}/2$, so the validity of the calculation begins to fail.

In this scenario, the measured abundance is approximately related to the unknown self-annihilation cross-section via

$$\Omega_{\rm DM} h^2 \simeq \frac{2 \times 2.4 \times 10^{-10}\,\mathrm{GeV}^{-2}}{\langle \sigma v \rangle_{\rm ann}}. \tag{5.1}$$

This is used with measurements of the DM abundance by Planck, $\Omega^{\rm obs}_{\rm DM} h^2 = 0.1199 \pm 0.0027$ [34], to find $\langle \sigma v \rangle_{\rm ann} \simeq 4.0 \times 10^{-9}\,\mathrm{GeV}^{-2}$ for thermal relic DM. This relation is only approximately accurate, and so we use the Micromegas code [49] to determine the coupling strength leading to the correct relic density for each model. We verified this technique against the semi-analytic technique outlined in e.g. Ref. [35].

If the DM mass lies at the electroweak scale, the thermal relic scenario provides a natural explanation for the observed DM density, and so the coupling strengths leading to the correct relic density are a natural benchmark with which to compare constraints from other DM searches, indicating the scale at which we expect the couplings may lie. However the relic density couplings should by no means be treated as a constraint. If the DM was

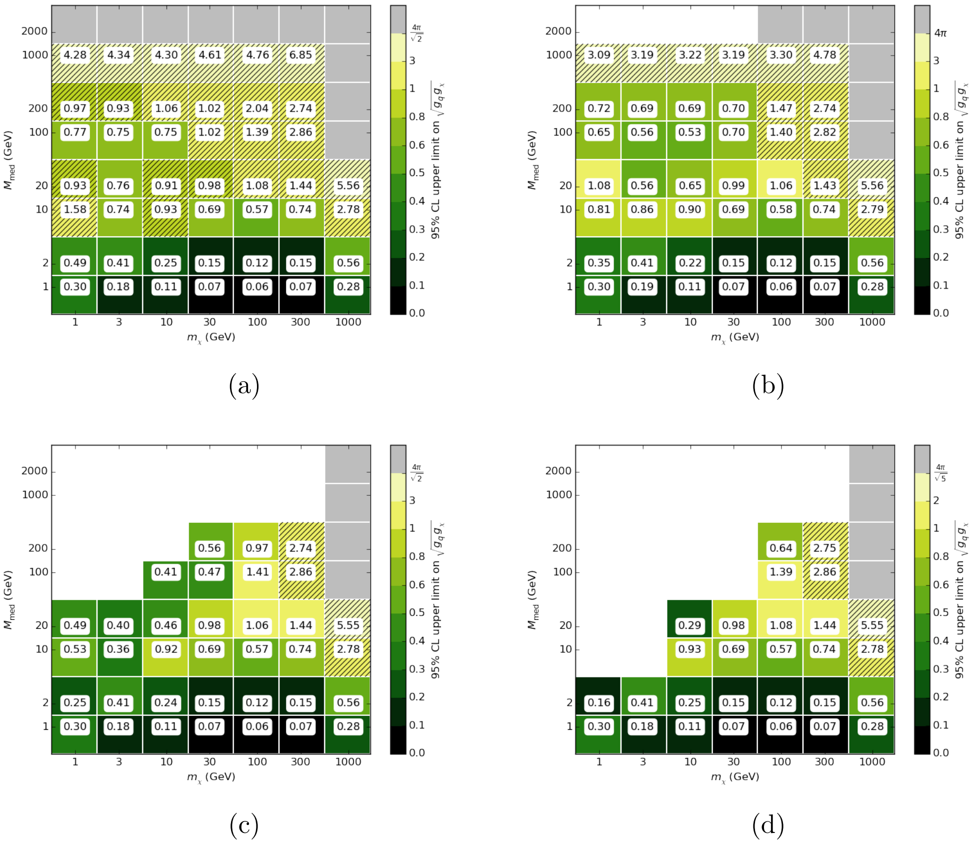

Figure 6: Upper limits on the coupling for the sA model, in the mono-Z channel, for $g_\chi/g_q = 0.5$ (a), 1 (b), 2 (c) and 5 (d). The grey region represents the phase space where no meaningful limit was obtained. The hatched region represents a limit which leads to a width greater than $M_{\text{med}}/2$, so the validity of the calculation begins to fail.

not produced thermally or if there is some unknown effect which modifies the evolution of the density with temperature, then these relations break down. Further, even if DM is a thermal relic, then the relationship no longer holds if there are other annihilation channels not taken into account, or if there are other beyond-SM particles contributing to the DM abundance.

5.2 Comparison with Direct Detection Constraints

Normally DD is better for vector and LHC is better for Axial vector, but in our case DD is better in both cases until you get to around $m_\chi = 5$ GeV at which point our interpolation has broken down.

5.3 Discussion

- Comparison to direct mediator searches: dijet gives strongest constraints on mediator especially for small r. Missing ET still good for large M but in this region EFT is fine

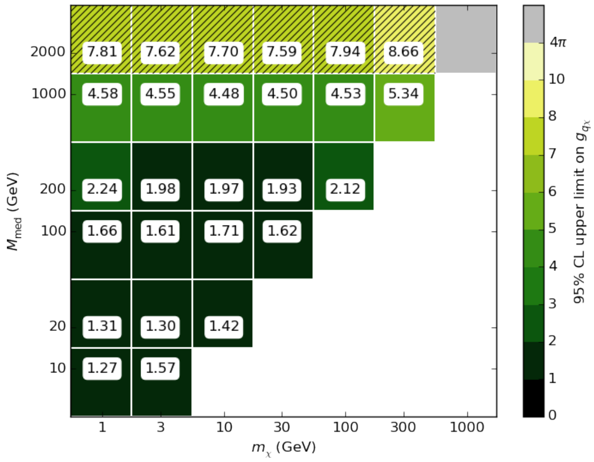

Figure 7: Upper limit on the coupling $g_{q\chi}$ for the tS model, in the mono-Z channel. The grey region represents the phase space where no meaningful limit was obtained. The hatched region represents a limit which leads to a width greater than $M_{\rm med}/2$, so the validity of the calculation begins to fail.

- Comparison to non-grid searches, e.g. McCullough et al
- Comparison to grid searches e.g. Zurek et al, Jacques and Nordstrom

MonoX searches dominate.

6 Acknowledgements

A Limit setting strategy

In this appendix we present a summary of the procedure employed to calculate the 95% confidence level (CL) limits on the coupling parameter $\sqrt{g_q g_\chi}$, where this parameter can be replaced with $g_{q\chi}$ for the tS model, and $M_\star$ in the validation of the mono-jet analysis.

A.1 Nominal Values

For each simplified model, the nominal value for the observed limit on the cross-section for the process $pp \to \mathrm{X} + \chi\bar{\chi}$ is calculated using the formula:

$$\sigma_{obs}^{lim}(pp \to \mathrm{X} + \chi\bar{\chi}) = \frac{N_{obs}}{\mathcal{L} \times \mathcal{A} \times \epsilon} \tag{A.1}$$

where N_{obs} is a calculated 95% CL upper limit on the number of signal events in the channel and signal region of interest; it is a model-independent quantity. $\mathcal{L}$ is the integrated luminosity, $\mathcal{A}$ is the acceptance (the fraction of signal events passing the channel/SR-specific selection criteria) and ϵ is the efficiency of the ATLAS detector for selecting channel/SR-specific signal events. For all channels the total luminosity is 20.3 fb^{-1} and $\mathcal{A}\times\epsilon$ is regarded as a single variable.

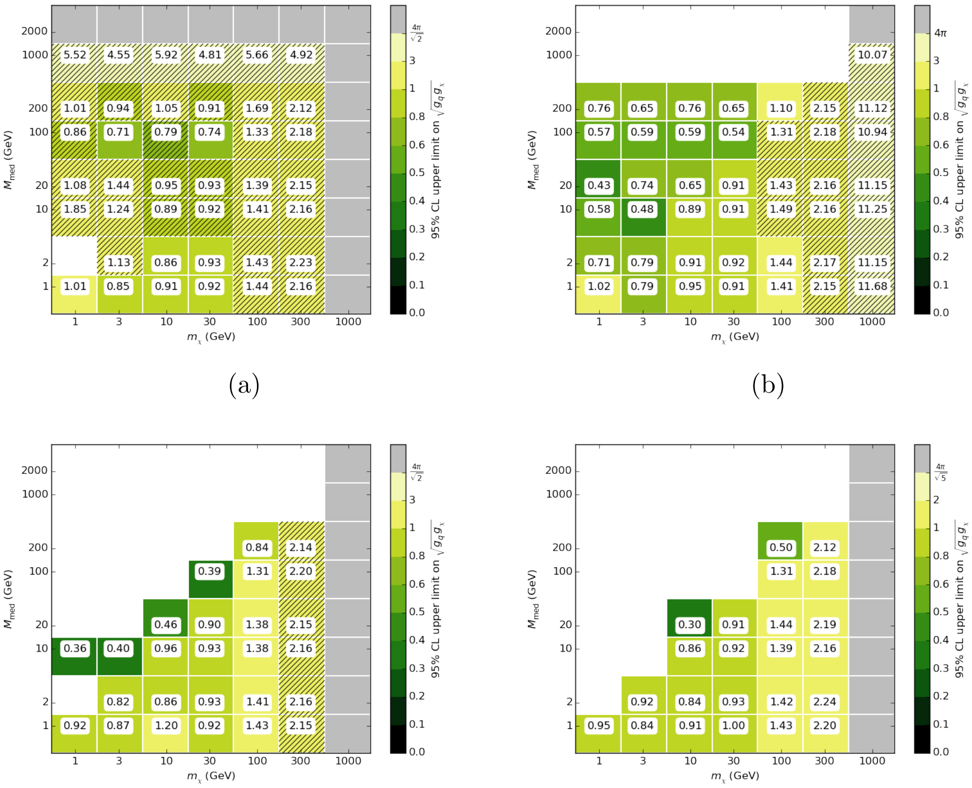

(a) (b) (c) (d)

Figure 8: Upper limits on the coupling for the sV model, in the mono-W/Z channel, for $g_\chi/g_q = 0.5$ (a), 1 (b), 2 (c) and 5 (d). The grey region represents the phase space where no meaningful limit was obtained. The hatched region represents a limit which leads to a width greater than $M_{\text{med}}/2$, so the validity of the calculation begins to fail. TO BE UPDATED WITH MONOWZ PLOTS.

In the following discussion, $\sqrt{g_q g_\chi}$ is assumed to also represent $g_{q\chi}$ from the tS model.

The nominal value for the observed limit Y, where Y is the suppression scale $M_\star$ in the validation of the mono-jet analysis, *or* the coupling values $\sqrt{g_q g_\chi}$ in the general case, is then calculated using

$$Y_{obs}^{lim} = Y^{gen} \left(\frac{\sigma_{obs}^{lim}}{\sigma^{gen}} \right)^{\frac{1}{4}} . \tag{A.2}$$

(Note: this section needs to be re-written to account for the on-shell case as well.)

The signal region in each case is chosen based on where the best 'expected' limit exists, where that limit is calculated assuming that exactly the expected SM background is observed.

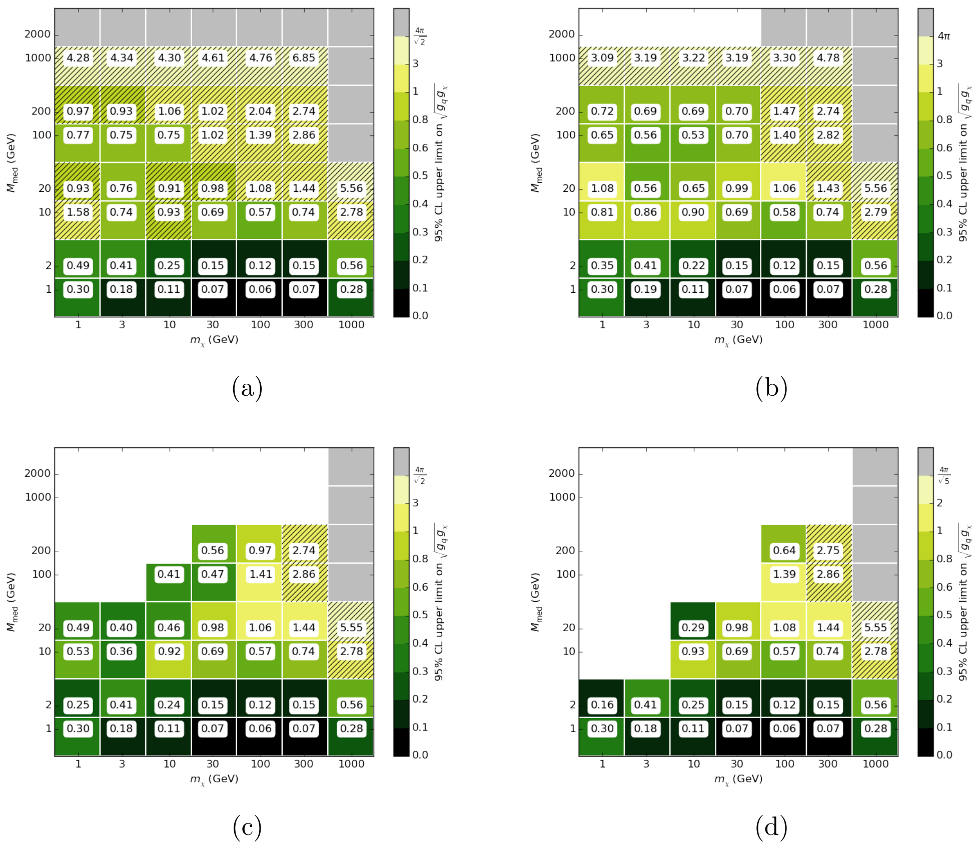

Figure 9: Upper limits on the coupling for the sA model, in the mono-W/Z channel, for $g_\chi/g_q = 0.5$ (a), 1 (b), 2 (c) and 5 (d). The grey region represents the phase space where no meaningful limit was obtained. The hatched region represents a limit which leads to a width greater than $M_{\rm med}/2$, so the validity of the calculation begins to fail. TO BE UPDATED WITH MONOWZ PLOTS.

A.2 Uncertainty Estimation

Our nominal limits on $M_\star$, $\sigma(pp \to X + \chi\bar{\chi})$ and $\sqrt{g_q g_\chi}$ rely on both σ_{gen} and $\mathcal{A} \times \epsilon$ and so are subject to systematic uncertainties which derive from our choice of MC generation procedure. For our MC samples, there are three key sources of systematic uncertainty: the factorisation and renormalisation scales, the strong coupling constant (α_s) and the parton distribution function (PDF).

Firstly, the factorisation and renormalisation default scales are varied simultaneously by factors of 2 ('up') and 0.5 ('down'). The systematic effects of the strong coupling constant and the PDF are difficult to separate and so are treated in tandem. We assume that the systematic uncertainty introduced by α_s at matrix-element level is negligible when compared to the PDF uncertainties, as demonstrated to be valid in Ref. [40]. The variation of α_s in conjunction with a PDF is done with the use of specific tunes in PYTHIA , which we change simultaneously with the PDF choice to estimate the uncertainty on $\Delta\sigma_{gen}$. The

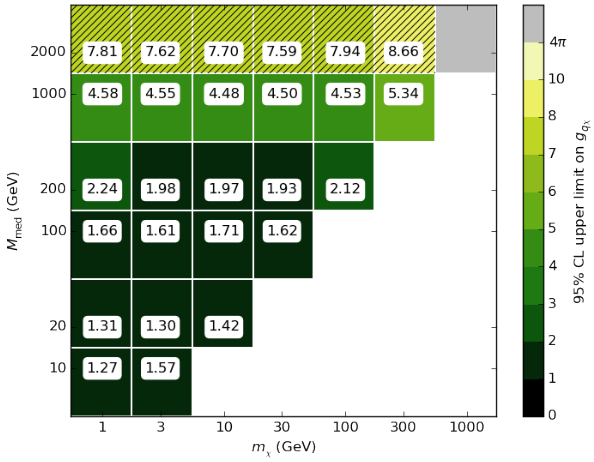

Figure 10: Upper limit on the coupling $g_{q\chi}$ for the tS model, in the mono-W/Z channel. The grey region represents the phase space where no meaningful limit was obtained. The hatched region represents a limit which leads to a width greater than $M_{\mathrm{med}}/2$, so the validity of the calculation begins to fail. TO BE UPDATED WITH MONOWZ PLOTS.

main systematic sources	PDF/tune	factorisation and renormalisation scales	matching scale (mono-jet only)
variation 'up'	NNPDF2.1LO + Monash tune	2	??
nominal	MSTW2008lo68cl + ATLAS UE AU2-MSTW2008LO	1	80 GeV
variation 'down'	CTEQ6L1 + ATLAS UE AU2-CTEQ6L1	0.5	??

Table 4: The sources of systematic uncertainty considered in this analysis. Each point in phase space is varied up or down by one of these sources, and the systematic uncertainty is taken to be the average difference in $\mathcal{A}'$ from the nominal value.

nominal choices of PDF and tune are varied 'up' to NNPDF2.1LO PDF + Monash tune, and 'down' to CTEQ6L1 PDF and ATLAS UE AU2-CTEQ6L1 tune. Millie: put discussion of matching scale systematic here. These systematic uncertainty sources are summarised in table 4.

Following eqns. A.1 and A.2, the relative uncertainty in the limit on $\sqrt{g_q g_\chi}$ (or on $M_\star$) is given by (to be updated with on-shell case also)

$$\frac{\Delta\sqrt{g_q g_\chi}}{\sqrt{g_q g_\chi}} = \frac{1}{4}\sqrt{\left(\frac{\Delta\sigma_{gen}}{\sigma_{gen}}\right)^2 + \left(\frac{\Delta(\mathcal{A}\times\epsilon)}{\mathcal{A}\times\epsilon}\right)^2 + \left(\frac{\Delta\mathcal{L}}{\mathcal{L}}\right)^2} \tag{A.3}$$

For $P = \sigma_{gen}, \mathcal{A}\times\epsilon$, the relative error $\Delta P/P$ is found by summing in quadrature the separate sources of uncertainty, according to

$$\left(\frac{\Delta P}{P}\right)^2_{\text{total}} = \left(\frac{\Delta P}{P}\right)^2_{\text{scale}} + \left(\frac{\Delta P}{P}\right)^2_{\text{PDF+tune}} + \left(\frac{\Delta P}{P}\right)^2_{\text{matching}} \tag{A.4}$$

where ΔP is taken as the average distance from the nominal value P when the systematic source is varied up and down. The statistical uncertainty is taken into account rather conservatively by using the 95%CL *lower* limit on $\mathcal{A}\times\epsilon$ as calculated with the Wald approximation, i.e. $\mathcal{A}\times\epsilon \to (\mathcal{A}\times\epsilon) - \Delta(\mathcal{A}\times\epsilon)$. The uncertainty on the luminosity is less than 3%, so is considered to be negligible in comparison to other systematic sources.

B Validation of signal simulation and event selection procedures

B.1 Monojet Channel

The MC generation and signal selection procedures for the mono-jet channel are validated via reproduction of the ATLAS limits on $M_\star \equiv M_{\text{med}}/\sqrt{g_q g_\chi}$, for the s-channel vector simplified model. A comparison of SR7 limits for a representative sample of mediator masses with $m_\chi = 50$ GeV, $\Gamma = M/8\pi$ and $\sqrt{g_q g_\chi} = 1$ is presented in Table 5. In general, good agreement is observed between the ATLAS and reproduced limits, with a maximum difference (with respect to the ATLAS limit) of <23%. We note that a discrepancy of a few percent is expected and allowed for three reasons. Firstly, the MC generation procedure employed in this analysis does not include a full simulation of the ATLAS detector. Instead, reconstruction effects are simulated by applying a Gaussian smearing of the jet p_{T} by a conservative factor of 5%. Next, the matching procedure employed in this analysis (and discussed in detail in Section 3.1.1) is largely simplified. This introduces a substantial uncertainty when compared to the matching procedure utilised by the ATLAS mono-jet group. For example, where the ATLAS group observe a maximum matching scale uncertainty of 5% for events with $E_{\text{T}}^{\text{miss}}$ above 350 GeV, we observe an uncertainty of $\sim$ 30%. Lastly, the 95% CL uncertainties on $M_\star$ for this work are estimated in a non-identical fashion to that used in the ATLAS analysis. In particular, where the ATLAS limits are estimated using the HistFitter package, we use the approach described in appendix A. As our results are consistently more conservative than those of the ATLAS analysis, we consider this approach acceptable.

B.2 Mono-Z Channel

The ATLAS mono-Z analysis result includes an upper limit on the coupling $g_{q\chi}$ for a t-channel simplified model that is very similar to the model investigated here, and so is used for validating our signal generation and selection procedure. The most significant

M [TeV]	$M_\star^{\mathrm{ATLAS95}}$ [GeV]	$M_\star^{95}$ [GeV]	Difference [%]
0.05	91	89	2.16
0.3	1151	1041	7.3
0.6	1868	1535	11.8
1	2225	1732	12.0
3	1349	1072	6.8
6	945	769	8.5
10	928	724	10.6
30	914	722	9.6

Table 5: Comparison of the 95% CL upper limits on $M_\star$ from this work ($M_\star^{95}$) and from the ATLAS mono-jet analysis ($M_\star^{\mathrm{ATLAS,95}}$) [39]. The values shown in the second and third columns are for the processes $pp \to j\chi\bar{\chi}$ and $pp \to jj\chi\bar{\chi}$ for the s-channel vector mediator model with $m_\chi = 50$ GeV, $\Gamma = M/8\pi$, $\sqrt{g_q g_\chi} = 1$ and QCUT = 80 GeV.

m_χ [GeV]	M_{med} [GeV]	$g_{q\chi}^{95\%\mathrm{CL}}$ (ATLAS)	$g_{q\chi}^{95\%\mathrm{CL}}$ (this work)	Difference [%]
10	200	1.9	2.0	5.3
	500	2.8	3.2	14.3
	700	3.5	4.4	25.7
	1000	4.5	5.2	15.6
200	500	3.4	4.0	17.6
	700	4.2	4.5	7.1
	1000	5.2	5.3	1.9
400	500	5.5	5.7	3.6
	700	6.1	6.5	6.6
	1000	7.2	7.4	2.8
1000	1200	23.3	24.1	3.4

Table 6: Comparison of the upper limit on $g_{q\chi}$ from the ATLAS analysis [45] and this work.

differences are in the number of mediating particles — the ATLAS model includes just two mediators (*up*- and *down*-type) compared to our six — and in the nature of the DM particle, which is taken to be Majorana. This latter choice does not impact the kinematic behaviour, but does scale the cross section by a simple factor. Additionally, while we use a universal coupling $g_{q\chi}$ to all three quark generations, the analysis used a model which set $g_{t,b\chi} = 0$.

Table 6 shows the 95% CL upper limits on $g_{q\chi}$ that we calculate using the same t-channel model and our own generation procedure (using the values in table **??**), compared with the limits on this same variable taken from the ATLAS analysis. The difference as a percentage of the ATLAS limit is also shown in the table. We see reasonable agreement; most of the 11 points in parameter space are within 10% of the ATLAS limits, and all are within 26%. Additionally, our results are consistently more conservative, which is to be expected due to the less sophisticated nature of our generation procedure. Similarly to the mono-jet validation, the dominant effects are due to the use of p_{T} smearing applied to the leptons, rather than considering the full reconstruction effects, and the simple systematic treatment that was used with HistFitter.

B.3 Mono-W/Z Channel

Johanna, please put your validation results here.

References

[1] ATLAS Collaboration, *Search for new phenomena with the monojet and missing transverse momentum signature using the ATLAS detector in $\sqrt{s}$ = 7 TeV proton-proton collisions*, *Phys. Lett. B* (2011), arXiv:1106.5327.

[2] ATLAS Collaboration, *Search for New Phenomena in Monojet plus Missing Transverse Momentum Final States using 10 fb^{-1} of pp collisions at $\sqrt{s}$=8 TeV with the ATLAS detector at the LHC*, 2012, ATLAS-CONF-2012-147.

[3] CMS Collaboration, *Search for new physics in monojet events in pp collisions at $\sqrt{s}$ = 8 TeV*, 2013, CMS-PAS-EXO-12-048.

[4] M. r. buckley, *Using effective operators to understand CoGeNT and CDMS-Si signals*, *Phys.Rev."* (2013), arXiv:1308.4146.

[5] J. Abdallah et al., *Search for new phenomena with mono-jet plus missing transverse energy signature in pp collisions at $\sqrt{s}$=8 TeV with the ATLAS detector*, 2012, ATL-COM-PHYS-2012-1211.

[6] N. Bell et al., *Searching for Dark Matter at the LHC with a Mono-Z*, *Phys.Rev.* (2012), arXiv:1209.0231.

[7] N. Zhou, D. Berge, and D. Whiteson, *Mono-everything: combined limits on dark matter production at colliders from multiple final states*, *Phys.Rev.* (2013), arXiv:1302.3619.

[8] M. Cahill-Rowley et al., *Complementarity and Searches for Dark Matter in the pMSSM*, 2013, arXiv:1305.6921.

[9] ATLAS Collaboration, *Further search for supersymmetry at $\sqrt{s} = 7$ TeV in final states with jets, missing transverse momentum and isolated leptons with the ATLAS detector*, *Phys.Rev.* (2012), arXiv:1208.4688.

[10] ATLAS Collaboration, *Search for squarks and gluinos with the ATLAS detector in final states with jets and missing transverse momentum using 4.7 fb^{-1} of $\sqrt{s} = 7$ TeV proton-proton collision data*, *Phys.Rev.* (2013), arXiv:1208.0949.

[11] ATLAS Collaboration, *Search for pair-produced third-generation squarks decaying via charm quarks or in compressed supersymmetric scenarios in pp collisions at $\sqrt{s} = 8$ TeV with the ATLAS detector*, *Phys.Rev.* (2014), arXiv:1407.0608.

[12] ATLAS Collaboration, *Search for squarks and gluinos with the ATLAS detector in final states with jets and missing transverse momentum using $\sqrt{s} = 8$ TeV proton-proton collision data*, *JHEP* (2014), arXiv:1405.7875.

[13] H. Dreiner et al., *Contact Interactions Probe Effective Dark Matter Models at the LHC*, *Europhys.Lett.* (2013), arXiv:1303.3348.

[14] J. Goodman et al., *Gamma Ray Line Constraints on Effective Theories of Dark Matter*, *Nucl.Phys.* (2011), arXiv:1009.0008.

[15] G. Busoni et al., *On the Validity of the Effective Field Theory for Dark Matter Searches at the LHC*, *Phys.Lett.* (2014), arXiv:1307.2253.

[16] Oliver Buchmueller, Matthew J. Dolan, Sarah A. Malik and Christopher McCabe, *Characterising dark matter searches at colliders and direct detection experiments: Vector mediators*, 2014, arXiv:1407.8257.

[17] J. Kumar and D. Marfatia. *Matrix element analyses of dark matter scattering and annihilation*, *Phys.Rev.* (2013), arXiv:1305.1611.

[18] G. Jungman et al., *Supersymmetric dark matter*, *Phys.Rept.* (1996).

[19] P. J. Fox et al., *Missing Energy Signatures of Dark Matter at the LHC*, *Phys.Rev.* (2012), arXiv:1109.4398.

[20] P. J. Fox, R. Harnik, R. Primulando, and C-T. Yu, *Taking a Razor to Dark Matter Parameter Space at the LHC*, *Phys.Rev.* (2012), arXiv:1203.1662.

[21] M. Papucci, A. Vichi, and K. M. Zurek, *Monojet versus rest of the world I: t-channel Models*, *JHEP* (2014), arXiv:1402.2285.

[22] Y. Bai, P. J. Fox, and R. Harnik, *The Tevatron at the Frontier of Dark Matter Direct Detection*, *JHEP* (2010), arXiv:1005.3797.

[23] J. Goodman et al., *Constraints on Dark Matter from Colliders*, *Phys.Rev.* (2010), arXiv:1008.1783.

[24] P. J. Fox, R. Harnik, J. Kopp, and Y. Tsai, *LEP Shines Light on Dark Matter*, *Phys.Rev.* (2011), arXiv:1103.0240.

[25] M. L. Graesser, I. M. Shoemaker, and L. Vecchi, *A Dark Force for Baryons*, 2011, arXiv:1107.2666.

[26] H. An and F. Gao, *Fitting CoGeNT Modulation with an Inelastic, Isopin-Violating Z' Model*, 2011, arXiv:1108.3943.

[27] CMS Collaboration, *Search for narrow resonances using the dijet mass spectrum in pp collisions at $\sqrt{s}$ = 8TeV*, *Phys.Rev.* (2013), arXiv:1302.4794.

[28] ATLAS Collaboration, *Search for high-mass resonances decaying to dilepton final states in pp collisions at s**(1/2) = 7-TeV with the ATLAS detector*, *JHEP* (2012), arXiv:1209.2535.

[29] P. Harris, V. V. Khoze, M. Spannowsky and C. Williams, *Constraining Dark Sectors at Colliders: Beyond the Effective Theory Approach*, *Phys.Rev.* (2015), arXiv:1411.0535.

[30] CMS Collaboration. *Search for new physics in monojet events in pp collisions at $\sqrt{s}$ = 8 TeV*, 2013, CMS-PAS-EXO-12-048.

[31] ATLAS Collaboration. *Search for New Phenomena in Monojet plus Missing Transverse*

Momentum Final States using 10 fb^{1} *of pp collisions at* $\sqrt{s} = 8$ *TeV with the ATLAS detector at the LHC*, 2012, ATLAS-CONF-2012-147.

[32] J. Kumar and D. Marfatia, *Matrix element analyses of dark matter scattering and annihilation*, *Phys.Rev.* (2013), arXiv:1305.1611.

[33] D. Alves et al., *Simplified Models for LHC New Physics Searches*, *J.Phys.* (2012), arXiv:1105.2838.

[34] P. A. R. Ade *et al.* [Planck Collaboration], Astron. Astrophys. **571**, A16 (2014) [arXiv:1303.5076 [astro-ph.CO]].

[35] G. Busoni, A. De Simone, T. Jacques, E. Morgante and A. Riotto, JCAP **1503**, no. 03, 022 (2015) [arXiv:1410.7409 [hep-ph]].

[36] CMS Collaboration. *Search for new physics in monojet events in pp collisions at* $\sqrt{s} = 8$ *TeV*, 2013, CMS-PAS-EXO-12-048.

[37] ATLAS Collaboration. *Search for New Phenomena in Monojet plus Missing Transverse Momentum Final States using 10 fb*^{1} *of pp collisions at* $\sqrt{s} = 8$ *TeV with the ATLAS detector at the LHC*, 2012, ATLAS-CONF-2012-147.

[38] ATLAS Collaboration. *Further search for supersymmetry at* $\sqrt{s} = 7$ *TeV in final states with jets, missing transverse momentum and isolated leptons with the ATLAS detector*, *Phys.Rev.* (2012), arXiv:1208.4688.

[39] ATLAS Collaboration. *Search for new phenomena in final states with an energetic jet and large missing transverse momentum in pp collisions at* $\sqrt{s} = 8$ *TeV with the ATLAS detector*, 2015, arXiv:1502.01518

[40] S. Schramm, *Searching for Dark Matter with the ATLAS Detector in Events with an Energetic Jet and Large Missing Transverse Momentum*, 2015, CERN-THESIS-2015-038.

[41] A. Cooper-Sarkar. *PDFs for the LHC*, 2011, arXiv:1107.5170.

[42] ATLAS Collaboration. *Search for dark matter candidates and large extra dimensions in events with a jet and missing transverse momentum with the ATLAS detector*, 2013, CERN-PH-EP-2012-210, arXiV:1210.4491.

[43] P. J. Fox et al. *Missing Energy Signatures of Dark Matter at the LHC*, *Phys. Rev.*, 2012.

[44] N. Bell, J. Dent, T. Jacques, and T. Weiler. *W/Z Bremsstrahlung as the Dominant Annihilation Channel for Dark Matter*, *Phys. Rev.*, 2011.

[45] ATLAS Collaboration. *Search for dark matter in events with a Z boson and missing transverse momentum in pp collisions at* $\sqrt{s} = 8$ *TeV with the ATLAS detector*, *Phys.Rev.D* ***90*** (2014) 012004, arXiv:1404.0051.

[46] J. Alwall /emphet al.. *The automated computation of tree-level and next-to-leading order differential cross sections, and their matching to parton shower simulations*, *JHEP07* (2014) 079, arXiv:1405.0301.

[47] A. D. Martin, W. J. Stirling, R. S. Thorne, G. Watt, *Parton distributions for the LHC*, *Eur.Phys.J.C63*, (2009), 189-285, arXiv:0901.0002.

[48] ATLAS Collaboration. *Summary of ATLAS Pythia8 tunes*, 2012, ATL-PHYS-PUB-2012-003.

[49] G. Blanger, F. Boudjema, A. Pukhov and A. Semenov, Comput. Phys. Commun. **192**, 322 (2015) doi:10.1016/j.cpc.2015.03.003 [arXiv:1407.6129 [hep-ph]].